Research Article Vol. 32, No. 3 / 29 Jan 2024 / Optics Express 2906
Optics EXPRESS

Arc discharge method to fabricate large concave structures for open-access fiber Fabry-Pérot cavities

DING FANG,[1,2,3] JIN-MING CUI,[1,2,3,4] WEI-BIN CHEN,[1,2,3] YAN CHEN,[1,2,3] RUI-RUI LI,[1,2,3] CHENG-HAO ZHANG,[1,2,3] YUN-FENG HUANG,[1,2,3,5] CHUAN-FENG LI,[1,2,3,6] AND GUANG-CAN GUO[1,2,3]

[1]*CAS Key Laboratory of Quantum Information, University of Science and Technology of China, Hefei 230026, China*
[2]*CAS Center For Excellence in Quantum Information and Quantum Physics, University of Science and Technology of China, Hefei 230026, China*
[3]*Hefei National Laboratory, University of Science and Technology of China, Hefei 230088, China*
[4]*jmcui@ustc.edu.cn*
[5]*hyf@ustc.edu.cn*
[6]*cfli@ustc.edu.cn*

Abstract: We present a novel micro-fabrication technique for creating concave surfaces on the endfacets of photonic crystal fibers. A fiber fusion splicer is used to generate arc discharges to melt and reshape the fiber endfacet. This technique can produce large spherical concave surfaces with roughness as low as 0.12 nm in various types of photonic crystal fibers. The deviation of fabricated surface and a spherical profile in the region of 70 μm in diameter is less than 50 nm. The center of the concave surface and the fiber mode field are highly coincident with a deviation less than 500 nm. Finesse measurements have shown that a Fabry-Pérot cavity composed of the fiber fabricated using this method and a plane mirror maintains finesse of 20000. This method is easy to replicate, making it a practical and efficient approach to fabricate concave surface on fibers for open-access fiber Fabry-Pérot cavities.

© 2024 Optica Publishing Group under the terms of the Optica Open Access Publishing Agreement

1. Introduction

An open-access fiber Fabry-Pérot cavity (FFPC) consists of two concave surfaces coated with high reflection coating on the endfacets of optical fibers. It has a small mode volume that greatly enhances the interaction between light and matter making it suitable for present a high-fidelity light-matter quantum interface [1]. Additionally, its short cavity length allows for full tunability of spatial and spectral degrees of freedom. Owing to the above advantages, FFPCs have been applied in various fields such as cavity quantum electrodynamics [2], optomechanics [3], sensing [4–6], nonlinear optics and more [7]. Different materials such as atoms [8–10], ions [11–14], NV-centers [15], SiV-centers [16], semiconductor quantum dots [17], carbon nanotubes [18] and others have been coupled to open-access FFPCs to build quantum network nodes or single photon sources. Moreover, FFPCs have also been used to construct wide-band tuning single-mode microlasers [19], scanning cavity microscopy [20] and optical fiber filters [21].

Various techniques have been employed to fabricate the concave surfaces for open-access FFPCs, including chemical etching [22], single-pulse CO_2 laser ablation [23–29], ion-beam milling [7,15] and laser written method [30]. These methods usually produce concave surfaces with small radius of curvature (ROC) or size, limiting the cavity length of high-finesse FFPCs due to the stability condition and clipping loss of the cavity. In some applications, it requires FFPCs with relatively long cavity lengths, for instance, the length of the FFPCs integrated in ion trap systems to couple ions with cavity modes are usually above 150 μm [13,14]. For atomic

#501532 https://doi.org/10.1364/OE.501532
Journal © 2024 Received 25 Jul 2023; revised 20 Oct 2023; accepted 3 Nov 2023; published 16 Jan 2024

Optics EXPRESS

systems, cavity length with several hundred micrometers allows elongated atomic ensembles to be placed in the cavity [31,32].

Using longer focal length lens to acquire larger beam waist when applying CO_2 laser ablation method can help enlarge the concave surface, but the boundary effect in the heat conduction process imposes a limit [24]. In order to further increase the concave size and ROC on the fiber endfacet, several multi-pulse laser ablation methods have been proposed [31,33,34]. Multi-pulse method have been able to process concave surfaces large enough to spread over the entire fiber endfacet by combining dozens of pulses, which allows the cavity length of open-access FFPCs to exceed 1.5 mm [31]. In addition, multi-pulse methods can also generate elliptical concave surfaces to construct FFPCs with engineered birefringence [35,36].

Although the multi-pulse method is capable of producing highly spherical concave surfaces covering the entire endfacet of the fiber, it imposes stringent requirements on the equipment as well as on the process parameters. The ablation process is highly nonlinear: a 1.2 percent power fluctuation can cause 10% to 15% change in depth of the concave surface for one single shot [24], which imposes stringent requirements on the power control of the pulses. The doping profile of the fiber, the angle between the fiber and the beam, the pulse duration, sequence and position all affect the ablation process, which makes adjusting experimental system and finding the optimal parameters challenging.

In this study, we propose a simpler approach to fabricating large concave surface on photonic crystal fiber (PCF) endfacets using a fiber fusion splicer. Fiber fusion splicer has been utilized to create in-fiber Fabry-Pérot cavity sensors [37,38] or combine different types of fibers together to match cavity mode with the mode field in the fiber [39]. Here we use a fiber fusion splicer to apply arc discharges on the fiber endfacet to reshape it into a concave surface. Compared to the multi-pulse ablation method, this method is simpler, more efficient, and easier to replicate. The concave surfaces fabricated are highly spherical and can reach 115 μm in diameter. The center of the concave surface and the fiber mode field are highly coincident, and the deviation between them is less than 500 nm. The roughness of concave surface is as low as 0.12 nm measured by AFM scanning. By adjusting the discharge duration and times, the ROC of the concave surface can be well controlled in a range. We had the fabricated LMA-8 fibers coated with an ion-beam sputtered (IBS) high-reflectivity coating for 650 nm. To evaluate the performance of the fabricated mirrors, we constructed a Fabry-Pŕot cavity consisting of a flat mirror and a fabricated fiber. The finesse of this cavity was measured to be as high as 20,000.

2. Arc discharge method

PCF is a special type of fiber characterized by a periodic array of air holes in the center, which can affect the propagation characteristics of light. The size of the air holes is comparable to the wavelength of light. PCFs can be classified into solid core and hollow core types, depending on whether the core is filled with air or not [40]. We employed a fiber fusion splicer (AI-7, Zhuoshi, China) to create large spherical structures on the endfacets of solid-core PCFs that can guide a single transverse mode over a wide range of wavelengths. Figure 1(a) shows the endfacet of the fiber. Different fibers have different photonic crystal sizes and cladding diameters, which result in different sizes and ROCs of concave surfaces after fabrication. We use three types of optical fibers: NKT LMA-5, LMA-8, and LMA-15, where the numbers represent their mode field diameters in microns. The cladding diameters for these fibers are 125 μm, 240 μm, and 230 μm respectively. To create the concave surface on the optical fiber endfacet using the arc discharge method, we followed these steps: The fibers with the coating layer removed are cut using a fiber cleaver (CT-106, Fujikura, Japan) to obtain a complete endfacet with an angle of less than 0.5 degrees. Then, we put the cut fiber into a fiber fusion splicer as Fig. 1(b) shows and set the discharge voltage and duration. Subsequently, the arc discharges generated by the splicer melted the silica and made the holes of the photonic crystal collapse. Multiple discharges

Optics EXPRESS

were conducted while observing surface deformation. The concave surface gradually formed over time due to surface tension as the discharge duration increased. The same effect can also be achieved with a single discharge of adequate discharge duration. Longer discharge duration, more discharges and higher discharge voltage all lead to an increase in the ROC of the concave surface.

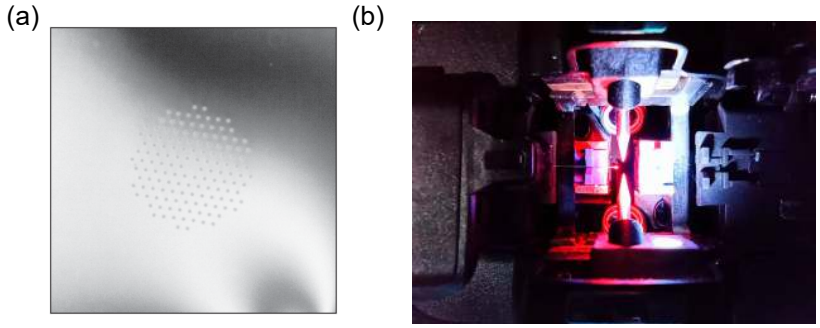

Fig. 1. (a) Photograph of the endfact of a LMA-8 fiber taken using a white light interference microscope. The black and white stripes in the figure reflect the undulations and slopes of the surface. (b) The optical fiber is attached to the stepper motor in the fusion splicer. After closing the cover of the fusion splicer, the stepper motor will advance the optical fiber into the work area and discharge it.

3. Large spherical structures

In a Fabry-Pérot cavity with finite size of the mirrors, some photons in the cavity are clipped at the edges of the mirrors and lost, which is called clipping loss. For a cavity consisting of two defined mirrors, the longer the length of the cavity, the larger the spot on the cavity mirror, corresponding to larger clipping loss. A rough estimation of clipping loss in open-access fiber Fabry-Pérot cavities has been proposed earlier [23]. Increasing the diameter of the concave mirrors is an effective way to reduce clipping loss. Our method allows large spherical concave surfaces to be fabricated on the endfacets of PCFs.

To observe changes in the surface shape with increasing discharge time, we applied 14 discharges to the endfacet of a LMA-8 fiber and scanned the surface with an optical profilometer after each discharge. Figure 2(a-c) illustrates the formation of concave surface during the discharge process and the discharge parameters are shown in Table 1. Since LMA series fibers are solid-type PCFs with a solid core, a small protrusion is created in the center as the hole area of the fiber begins to collapse. As the number or duration of discharges increases, the protrusion in the center disappears under surface tension and eventually forms a highly spherical concave surface.

Table 1. Discharge parameters used in the test

Fiber-type	Duration/ms	Voltage/mV	Number of discharges	ROC of the concave surface/μm	Diameter of the concave surface/μm
LMA-8	1400	600	14	289	90
LMA-15	1400	1100	1	557	115

We fabricated a concave surface on the endfacet of a LMA-15 fiber using a single discharge with longer duration. To obtain the ROC and eccentricity of the concave surface, a set of cross-sectional profiles was captured across the center of the concave surface, perpendicular

Optics EXPRESS

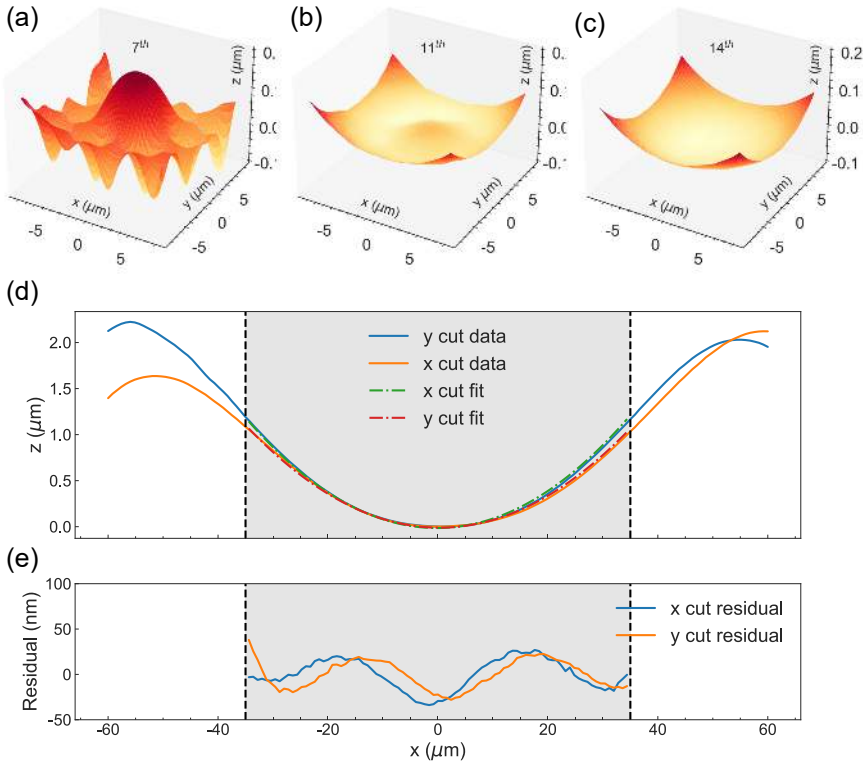

Fig. 2. Concave surface analysis. (a) Shape of the concave mirror on a LMA-8 fiber after seven, (b) eleven, (c) and fourteen discharges. (d) Cross-sectional profiles of the concave surface on the endfacet of a LMA-15 fiber and corresponding circle-curve fits on a circular region with a diameter of 70 μm. (e) Fitting residuals.

to each other. Circle-curve fitting was employed to determine the profiles' ROCs. In order to find the minor and major axes of the concave surface, we rotated the direction to capture cross-sectional profiles six times and found the set with the largest difference in ROCs between the two profiles. Figure 2(d,e) displays the cross-sectional profiles, exhibiting ROCs measuring 557 μm along the major axis and 504 μm along the minor axis. Eccentricity can be calculated by $\varepsilon = \sqrt{1 - R_{\text{min}}/R_{\text{max}}}$, where R_{min} and R_{max} are the estimated ROCs along the minor and major axes. With this method, we find an averaged eccentricity of 0.29 ± 0.02 among 5 samples.

The entire concave surface can reach 115 μm in diameter and maintains an highly spherical shape within its center diameter of 70 μm, a region where the residuals of the circle-curve fit do not exceed 70 nm. Compared with the Gaussian profile of the depression generated by single pulse laser ablation method, a spherical concave surface has a relatively larger effective mirror diameter [31], and there is less finesse decrease at specified cavity length caused by resonant mode mixing that originates from the non-spherical overall shape of the concave structure [41].

4. Controllable ROC over a wide range

The ROC of the concave surface can be flexibly adjusted by manipulating the discharge parameters and number of discharges. In order to study the variation of the surface ROC during the discharge process, we discharged a fiber multiple times with short discharge duration and measured the surface ROC after each discharge.

Optics EXPRESS

Figure 3(a) shows how the ROC of the concave surface changes during the fabrication of LMA-15 fibers with different numbers of discharges. We fitted the profiles within 60 μm diameter regions at the center using the method mentioned earlier and plotted the standard deviation as error bars. We performed the same test for LMA-5 fiber, a 24 μm diameter region is used for fitting because the concave surface is smaller and the result is shown in Fig. 3(b). The two PCFs have air hole arrays with similar shape but different sizes. The diameter of the air hole array at the center of LMA-5 fiber is approximately 40 μm, while that of LMA-15 fiber is 120 μm. The ROCs of the concave surfaces on both fibers increase consistently with cumulative discharge duration. The main difference between the concave surfaces fabricated with the two fibers is their size and lower limit of ROC. The larger the photonic crystal of the fiber, the larger the ROC and size of the concave surface.

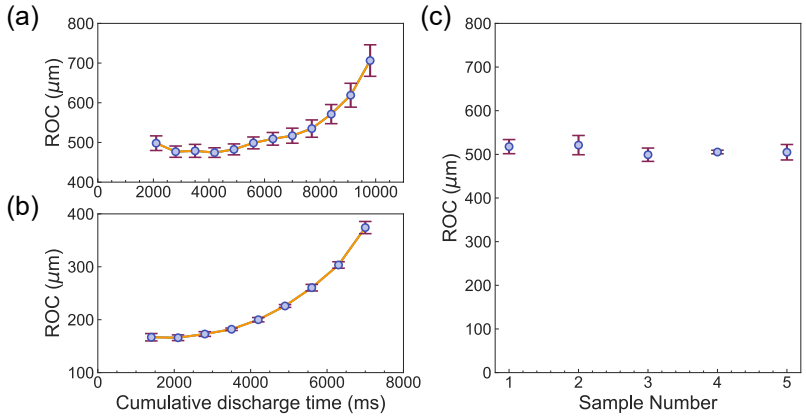

Fig. 3. The ROC of the concave surface increases with the cumulative discharge duration. (a) When fabricating the LMA-15 fiber, the discharge voltage was set to 1200 mV, and each discharge lasted 700 ms. The error bars represent the standard deviations of the ROCs given by fitting on four different cross-sectional profiles. (b) When fabricating the LMA-15 fiber, the discharge voltage is set to 700 mV and the duration of each discharge is set to 700 ms. (c) The ROCs of concave surfaces obtained from the repeated fabrication of five LMA-15 fibers. The discharge voltage used for fabricating was 1400 mV and the discharge duration was 800 ms.

To verify the controllability of the ROCs of the fabricated concave surfaces, we repeated the experiment with five LMA-15 fibers using the same discharge parameters and showed the ROCs of the concave surfaces in Fig. 3(c). The results show that our method has good reproducibility, the deviation of the ROCs obtained from five repetitions is less than 5%. It should be noted that the remaining battery charge of the fusion splicer may affect the discharge voltage. Therefore, it is crucial to keep the power supply connected during fabrication to obtain controlled ROCs of the concave surfaces.

5. Surface roughness

The roughness of the concave surface is an important indicator for quality of the cavity mirror, and the loss due to scattering on the cavity mirror can be estimated by Eq. (1) [23].

$$\mathcal{L}_s \approx (4\pi\sigma/\lambda)^2, \tag{1}$$

where σ refers to the surface roughness and λ is the light wavelength.

We measured the roughness of the fabricated concave surface on a LMA-8 fiber using atomic force microscopy (AFM). We scanned areas of 1×1 μm^2 and 5×5 μm^2 in the center of the

Optics EXPRESS

concave surface, as shown in Fig. 4(a). To eliminate the effect of large-scale shapes, we used the deviation from a polynomial fit for roughness calculation. Figure 4(b) shows the 2D Power Spectral Density (PSD) of the AFM scan result. The PSD provides a representation of the amplitude of a surface's roughness as a function of the spatial frequency. It also contains statistical information that is unbiased by the particular scan size and pixel resolution chosen by the researcher. The tapered PSD as shown in the figure indicates a flat, isotropic surface [42]. The root-mean-square roughness (Rq) and average roughness (Ra) for the 1 μm area were 0.16 nm and 0.13 nm, respectively. For the 5 μm area, R_q and R_a were 0.19 nm and 0.15 nm.

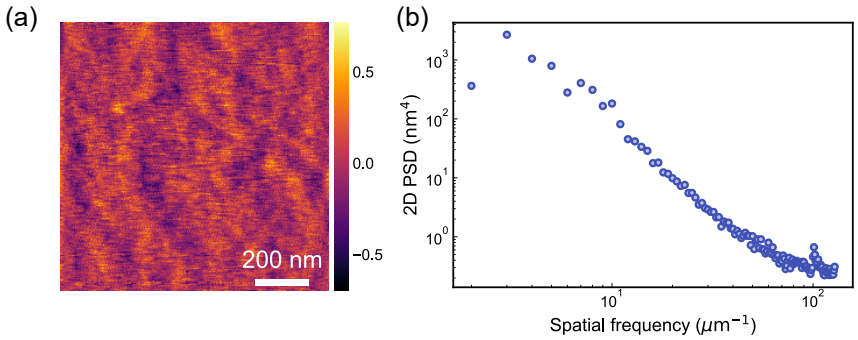

Fig. 4. (a) An AFM measurement of a 1×1 μm^2 area of the mirror surface with a 6-order polynomial fit subtracted from the original data. (b) 2D power spectral density of the remaining height elevation obtained from the AFM scan.

Surface roughness obtained from height scan of AFM contains scan noise. To estimate scan noise, we scanned a 1 μm region of V-1 mica sheet (Ted Pella), which is often used as a substrate for AFM measurements due to its low roughness. The scan result showed a mean square roughness of 0.11 nm and an average roughness of 0.08 nm for the mica sheet. Correcting for this according to the error propagation function yields R_q=0.12 nm, R_a=0.10 nm for 1 μm area, and R_q=0.15 nm, R_a=0.13 nm for 5 μm area. The roughness values for the concave surface are lower than those reported in previous studies (R_q=0.2 nm) [24,28,31]. Using Eq. (1), we estimated the scattering loss $\mathcal{L}_s$ to be approximately 8 ppm for a light wavelength of 650 nm.

6. Deviation between concave surface and fiber mode field

In a fiber cavity consisting of two fibers, the misalignment of the two fibers and the deviation of the concave surface from the center of the fiber both affect the angle and position of the cavity mode, leading to a decrease in the coupling efficiency between the cavity mode and the fiber mode. For a specific fiber cavity, the degradation of coupling efficiency due to angular and positional deviations can be estimated [20].

Due to the good symmetry of the photonic crystal structure, the concave surface fabricated by the arc discharge method and the mode field at the center of the fiber are highly coincident. To evaluate the deviation between them, we used an interference objective to observe the fiber endfacet and identify the center of the concave surface. First, we altered the objective lens and fiber's distance to make the interference at the concave center destructive. Then we coupled a laser to the other end of the fiber. Figure 5(a) shows the photo taken through the interference objective, where the highlighted area in the center is the outgoing laser indicating the mode field, and the surrounding interference circles reflect the position of the concave surface.

To calculate the deviation between the concave center and the mode field of the fiber, we chose a pair of perpendicular axes that crossed at the concave center. Then we plotted the light intensity distribution curves along the two axes, as shown in Fig. 5(b). We use Gaussian functions to fit

Optics EXPRESS

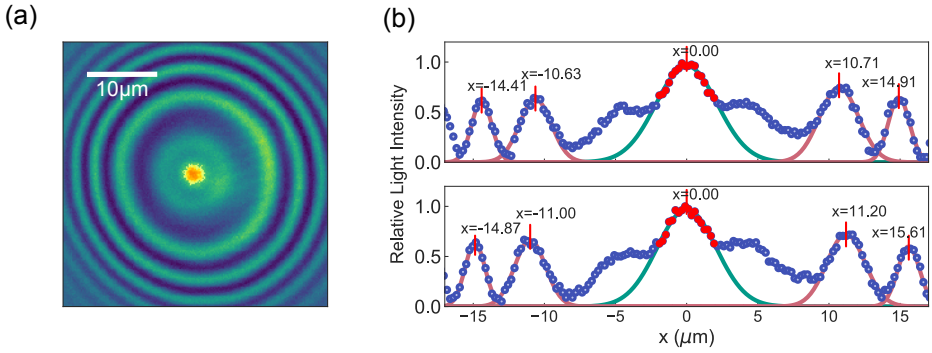

Fig. 5. (a) Interference pattern of the concave mirror (color map with blue-yellow) and the outgoing laser indicated mode field of the fiber (color map with red). (b) Light intensity distribution along two perpendicular axes passing through the center. The blue dots show the measured light intensity, the green curve is a Gaussian fit for the central bright spot, the red dots denote fitting points, and the purple curves represent Gaussian fits for the surrounding bright rings.

the peaks in the figure and obtain their position coordinates. The central peak corresponds to the outgoing laser, and the side peaks corresponds to the bright rings in the interference pattern. The coordinates of the mode field are specified as $x_0 = 0$, then the deviation between the mode field of the fiber and concave mirror center can be expressed as $\delta x = (x_+ + x_-)/2$, where x_+ and x_- are coordinates of side peaks. Similarly, the deviation perpendicular to this direction is defined as δy. Then the total deviation between the concave surface center and the fiber mode field is $\Delta = \sqrt{\delta x^2 + \delta y^2}$. The interference pattern within 35 μm around the central bright spot are selected as valid data. We rotated the axes six times and repeated the calculations to obtain the mean values and standard deviations of the deviations. The deviation between the concave center and the mode field of the fiber was estimated to be 0.44 ± 0.19 μm.

7. Cavity characterization via finesse measurements

After fabrication, the fiber surfaces were coated with a high reflectivity coating at 650 nm by LaserOptics. A plane mirror and a LMA-8 fiber with same coating are used to build a Fabry-Pérot cavity. The quality of an optical cavity is characterizes by its finesse, given by

$$\mathcal{F} = \frac{2\pi}{\mathcal{L}_A + \mathcal{L}_s + \mathcal{L}_{cl} + \mathcal{T}}, \tag{2}$$

where $\mathcal{L}_A$ is the total absorption loss on the two mirrors in the coatings. It is about 75 ppm on each mirror according to LaserOptics. $\mathcal{L}_s$ is the total scattering loss and $\mathcal{T}$ is the total transmission. The nominal transmission for one mirror at 650 nm is 50±30 ppm. $\mathcal{L}_{\mathrm{cl}}$ represents the clipping loss. Each term representing the sum of the contributions of the two mirrors. The coating typically determines the absorption loss and transmission, whereas the clipping loss is primarily dependent on the cavity length and the mirror size, and scattering loss is related to the roughness of the reflective surfaces.

The mirror surface on the fiber endfacet was scanned using a profilometer, and 2D spherical fit gave a ROC of 303 μm. The variation of finesse with cavity length was measured by mounting the plane mirror on a one-dimensional piezoelectric translation stage (PI P-628). Ten measurements were taken at different locations of the plane mirror to prevent local variations of the mirror coating from influencing the result. The average of the ten measurements was then plotted in Fig. 6. The blue line shows the variation of finesse with cavity length, and the red area represents

Optics EXPRESS

the error band coming from the standard deviation of the finesse in ten measurements. The variation of finesse was measured over a range of cavity lengths from 0 to 250 μm. For cavity lengths below 100 μm, the finesse remained stable at approximately 20000. However, at 110 μm, a small decrease in finesse was observed. This is caused by the fact that the entire fiber endfacet is not perfectly spherical, which results in the coupling of the fundamental mode and higher order modes at certain cavity length.

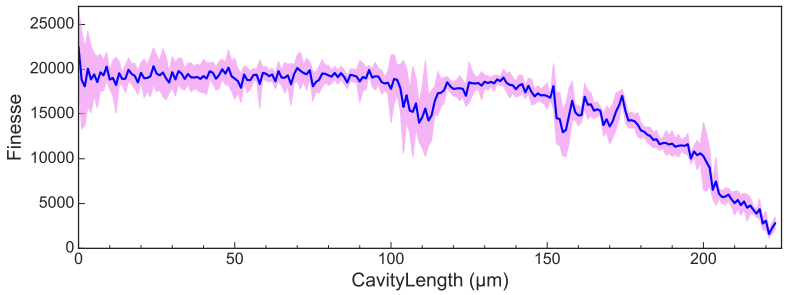

Fig. 6. Variation of finesse with cavity length in a Fabry-Pérot cavity composed of a plane mirror and fabricated LMA-8 fiber, the ROC of the concave surface on the fiber endfacet is 303 μm.

8. Conclusions

In this paper, we describe arc discharge method to fabricate concave mirrors on the endfacets of PCFs. Compared with the CO_2 laser ablation method, which requires complicated design and precise control of the pulse duration, laser power, beam position and pulse sequence, our approach greatly improves production efficiency, simplifies the steps, and reduces processing time and equipment requirements. Using a fiber fusion splicer, we fabricate a large spherical concave surface with controllable ROC and low roughness on the fiber endfacet. The center of the concave surface is highly coincident with the fiber mode field. The Fabry-Pérot cavity consisting of a coated fiber and a plane mirror shows satisfactory optical transmission characteristics. The finesse of the cavity can reach 20000 and hardly decreases when the cavity length is extended up to one-third of the concave surface's ROC. Our method offers a new perspective on fabricated concave surface on optical fibers utilized in open-access fiber cavities. In addition, this method can be used not only for fabricating concave surfaces on flat PCF endfacet, but also for extending the ROC of existing concave surface. It may be possible to make this method also applicable to single-mode and multi-mode fibers by first processing some microstructure or fuse a section of PCF to the fiber tip.

Funding. Innovation Program for Quantum Science and Technology (2021ZD0301200, 2021ZD0301604); Key Research Program of Frontier Science, Chinese Academy of Sciences (QYZDY-SSWSLH003); Science Foundation of Chinese Academy of Sciences (ZDRW-XH-2019-1); National Natural Science Foundation of China (11734015, 11774335); Fundamental Research Funds for the Central Universities (WK2470000027, WK2470000028, ZDRW-XH-2019-1); National Key Research and Development Program of China (2017YFA0304100); Students Innovation and Entrepreneurship Foundation of USTC (XY2022G11).

Acknowledgments. This work was partially carried out at the USTC Center for Micro and Nanoscale Research and Fabrication.

Disclosures. The authors declare no conflicts of interest.

Data availability. Data underlying the results presented in this paper are not publicly available at this time but may be obtained from the authors upon reasonable request.

References

Optics EXPRESS

1. M. Brekenfeld, D. Niemietz, J. D. Christesen, and G. Rempe, "A quantum network node with crossed optical fibre cavities," Nat. Phys. **16**(6), 647–651 (2020).
2. J. Miguel-Sánchez, A. Reinhard, E. Togan, T. Volz, A. Imamoglu, B. Besga, J. Reichel, and J. Estève, "Cavity quantum electrodynamics with charge-controlled quantum dots coupled to a fiber Fabry-Perot cavity," New J. Phys. **15**(4), 045002 (2013).
3. N. E. Flowers-Jacobs, S. W. Hoch, J. C. Sankey, A. Kashkanova, A. M. Jayich, C. Deutsch, J. Reichel, and J. G. E. Harris, "Fiber-cavity-based optomechanical device," Appl. Phys. Lett. **101**, (2012).
4. C. Saavedra, D. Pandey, W. Alt, D. Meschede, and H. Pfeifer, "Spectroscopic gas sensor based on a fiber Fabry-Perot cavity," Phys. Rev. Appl. **18**(4), 044039 (2022).
5. X.-X. Gao, J.-M. Cui, M.-Z. Ai, Y.-F. Huang, C.-F. Li, and G.-C. Guo, "An acoustic sensor based on active fiber Fabry-Perot microcavities," Sensors **20**(20), 5760 (2020).
6. F. G. Cervantes, L. Kumanchik, J. Pratt, and J. M. Taylor, "High sensitivity optomechanical reference accelerometer over 10 kHz," Appl. Phys. Lett. **104**(22), 221111 (2014).
7. H. Pfeifer, L. Ratschbacher, J. Gallego, C. Saavedra, A. Faßbender, A. von Haaren, W. Alt, S. Hofferberth, M. Köhl, S. Linden, and D. Meschede, "Achievements and perspectives of optical fiber Fabry-Perot cavities," Appl. Phys. B **128**(2), 29 (2022).
8. J. Gallego, W. Alt, T. Macha, M. Martinez-Dorantes, D. Pandey, and D. Meschede, "Strong Purcell Effect on a neutral atom trapped in an open fiber cavity," Phys. Rev. Lett. **121**(17), 173603 (2018).
9. M. Uphoff, M. Brekenfeld, G. Rempe, and S. Ritter, "An integrated quantum repeater at telecom wavelength with single atoms in optical fiber cavities," Appl. Phys. B **122**(3), 46 (2016).
10. C. Junge, D. O'Shea, J. Volz, and A. Rauschenbeutel, "Strong coupling between single atoms and nontransversal photons," Phys. Rev. Lett. **110**(21), 213604 (2013).
11. M. Teller, V. Messerer, K. Schüppert, Y. Zou, D. A. Fioretto, M. Galli, P. C. Holz, J. Reichel, and T. E. Northup, "Integrating a fiber cavity into a wheel trap for strong ion–cavity coupling," AVS Quantum Sci. **5**(1), 012001 (2023).
12. H. Takahashi, E. Kassa, C. Christoforou, and M. Keller, "Strong coupling of a single ion to an optical cavity," Phys. Rev. Lett. **124**(1), 013602 (2020).
13. T. G. Ballance, H. M. Meyer, P. Kobel, K. Ott, J. Reichel, and M. Köhl, "Cavity-induced backaction in Purcell-enhanced photon emission of a single ion in an ultraviolet fiber cavity," Phys. Rev. A **95**(3), 033812 (2017).
14. B. Brandstätter, A. McClung, K. Schüppert, *et al.*, "Integrated fiber-mirror ion trap for strong ion-cavity coupling," Rev. Sci. Instrum. **84**(12), 123104 (2013).
15. R. Albrecht, A. Bommer, C. Pauly, F. Mücklich, A. W. Schell, P. Engel, T. Schröder, O. Benson, J. Reichel, and C. Becher, "Narrow-band single photon emission at room temperature based on a single nitrogen-vacancy center coupled to an all-fiber-cavity," Appl. Phys. Lett. **105**(7), 073113 (2014).
16. S. Häußler, J. Benedikter, K. Bray, B. Regan, A. Dietrich, J. Twamley, I. Aharonovich, D. Hunger, and A. Kubanek, "Diamond photonics platform based on silicon vacancy centers in a single-crystal diamond membrane and a fiber cavity," Phys. Rev. B **99**(16), 165310 (2019).
17. B. Besga, C. Vaneph, J. Reichel, J. Estève, A. Reinhard, J. Miguel-Sánchez, A. Imamoğlu, and T. Volz, "Polariton boxes in a tunable fiber cavity," Phys. Rev. Appl. **3**(1), 014008 (2015).
18. A. Jeantet, Y. Chassagneux, C. Raynaud, P. Roussignol, J. Lauret, B. Besga, J. Estève, J. Reichel, and C. Voisin, "Widely tunable single-photon source from a carbon nanotube in the Purcell regime," Phys. Rev. Lett. **116**(24), 247402 (2016).
19. X.-X. Gao, J.-M. Cui, Z.-H. Hu, C.-H. Dong, J. Wang, Y.-F. Huang, C.-F. Li, and G.-C. Guo, "Fast and wide-band tuning single-mode microlaser based on fiber Fabry-Perot microcavities," Photonics Res. **8**(10), 1642 (2020).
20. M. Mader, J. Reichel, T. W. Hänsch, and D. Hunger, "A scanning cavity microscope," Nat. Commun. **6**(1), 7249 (2015).
21. B. Zhou, H. Jiang, R. Wang, and C. Lu, "Optical fiber Fabry-Perot filter with tunable cavity for high-precision resonance wavelength adjustment," J. Lightwave Technol. **33**, 2905–2954 (2015).
22. P. Qing, J. Gong, X. Lin, N. Yao, W. Shen, A. Rahimi-Iman, W. Fang, and L. Tong, "A simple approach to fiber-based tunable microcavity with high coupling efficiency," Appl. Phys. Lett. **114**(2), 021106 (2019).
23. D. Hunger, T. Steinmetz, Y. Colombe, C. Deutsch, T. W. Hänsch, and J. Reichel, "A fiber Fabry-Perot cavity with high finesse," New J. Phys. **12**(6), 065038 (2010).
24. D. Hunger, C. Deutsch, R. J. Barbour, R. J. Warburton, and J. Reichel, "Laser micro-fabrication of concave, low-roughness features in silica," AIP Adv. **2**(1), 012119 (2012).
25. T. Ruelle, M. Poggio, and F. Braakman, "Optimized single-shot laser ablation of concave mirror templates on optical fibers," Appl. Opt. **58**(14), 3784 (2019).
26. L. Greuter, S. Starosielec, D. Najer, A. Ludwig, L. Duempelmann, D. Rohner, and R. J. Warburton, "A small mode volume tunable microcavity: Development and characterization," Appl. Phys. Lett. **105**(12), 121105 (2014).
27. M. Uphoff, M. Brekenfeld, G. Rempe, and S. Ritter, "Frequency splitting of polarization eigenmodes in microscopic Fabry-Perot cavities," New J. Phys. **17**(1), 013053 (2015).
28. A. Muller, E. B. Flagg, J. R. Lawall, and G. S. Solomon, "Ultrahigh-finesse, low-mode-volume Fabry-Perot microcavity," Opt. Lett. **35**(13), 2293 (2010).

Optics EXPRESS

29. K. Zhou, J.-M. Cui, Y.-F. Huang, Z. Wang, Z.-H. Qian, Q.-M. Wu, J. Wang, R. He, W.-M. Lv, C.-K. Hu, Y.-J. Han, C.-F. Li, and G.-C. Guo, "An ultraviolet fiber Fabry-Perot cavity for florescence collection of trapped ions," Chin. Phys. Lett. **34**(1), 013701 (2017).
30. J. Hessenauer, K. Weber, J. Benedikter, T. Gissibl, J. Höfer, H. Giessen, and D. Hunger, "Laser written mirror profiles for open-access fiber Fabry-Perot microcavities," Opt. Express **31**(11), 17380 (2023).
31. K. Ott, S. Garcia, R. Kohlhaas, K. Schüppert, P. Rosenbusch, R. Long, and J. Reichel, "Millimeter-long fiber Fabry-Perot cavities," Opt. Express **24**(9), 9839 (2016).
32. M.-Z. Huang, J. A. de la Paz, T. Mazzoni, K. Ott, P. Rosenbusch, A. Sinatra, C. L. G. Alzar, and J. Reichel, "Observing spin-squeezed states under spin-exchange collisions for a second," PRX Quantum **4**(2), 020322 (2023).
33. H. Takahashi, J. Morphew, F. Oručević, A. Noguchi, E. Kassa, and M. Keller, "Novel laser machining of optical fibers for long cavities with low birefringence," Opt. Express **22**(25), 31317 (2014).
34. J. Gallego, S. Ghosh, S. K. Alavi, W. Alt, M. Martinez-Dorantes, D. Meschede, and L. Ratschbacher, "High-finesse fiber Fabry-Perot cavities: stabilization and mode matching analysis," Appl. Phys. B **122**(3), 47 (2016).
35. S. Garcia, F. Ferri, K. Ott, J. Reichel, and R. Long, "Dual-wavelength fiber Fabry-Perot cavities with engineered birefringence," Opt. Express **26**(17), 22249 (2018).
36. J.-M. Cui, K. Zhou, M.-S. Zhao, M.-Z. Ai, C.-K. Hu, Q. Li, B.-H. Liu, J.-L. Peng, Y.-F. Huang, C.-F. Li, and G.-C. Guo, "Polarization nondegenerate fiber Fabry-Perot cavities with large tunable splittings," Appl. Phys. Lett. **112**(17), 171105 (2018).
37. K. Zhou, M.-Z. Ai, Z.-H. Qian, X.-X. Gao, Z.-H. Hu, Q. Li, L. Yuan, Z. Wang, Y.-F. Huang, T. Tu, J.-M. Cui, C.-F. Li, and G.-C. Guo, "High-sensitivity strain sensor with an in-fiber air-bubble Fabry-Perot interferometer," Appl. Phys. Lett. **113**(18), 181901 (2018).
38. G. K. B. Costa, P. M. P. Gouvêa, L. M. B. Soares, J. M. B. Pereira, F. Favero, A. M. B. Braga, P. Palffy-Muhoray, A. C. Bruno, and I. C. S. Carvalho, "In-fiber Fabry-Perot interferometer for strain and magnetic field sensing," Opt. Express **24**(13), 14690 (2016).
39. G. K. Gulati, H. Takahashi, N. Podoliak, P. Horak, and M. Keller, "Fiber cavities with integrated mode matching optics," Sci. Rep. **7**(1), 5556 (2017).
40. J. Haus, "Nanophotonic devices," in *Fundamentals and Applications of Nanophotonics*, International Society for Optics and Photonics, (2016), pp. 341–395.
41. J. Benedikter, T. Hümmer, M. Mader, B. Schlederer, J. Reichel, T. W. Hänsch, and D. Hunger, "Transverse-mode coupling and diffraction loss in tunable Fabry-Perot microcavities," New J. Phys. **17**(5), 053051 (2015).
42. NanoScope, Power Spectral Density (PSD) (2010). https://www.nanophys.kth.se/ nanolab/afm/icon/bruker-help/Content/SoftwareGuide/Offline/AnalysisFunct/PowerSpectralDens.htm.

194.84.129.[illegible] (2024-09-02 09:50:21)